High Voltage $LiNi_{0.5}Mn_{0.3}Co_{0.2}O_2$/Graphite Cell Cycled at 4.6 V with a FEC/HFDEC-Based Electrolyte

*Meinan He, Chi-Cheung Su, Zhenxing Feng, Li Zeng, Tianpin Wu, Michael J. Bedzyk, Paul Fenter, Yan Wang, and Zhengcheng Zhang**

A high voltage $LiNi_{0.5}Mn_{0.3}Co_{0.2}O_2$/graphite cell with a fluorinated electrolyte formulation 1.0 M $LiPF_6$ fluoroethylene carbonate/bis(2,2,2-trifluoroethyl) carbonate is reported and its electrochemical performance is evaluated at cell voltage of 4.6 V. Comparing with its nonfluorinated electrolyte counterpart, the reported fluorinated one shows much improved Coulombic efficiency and capacity retention when a higher cut-off voltage (4.6 V) is applied. Scanning electron microscopy/energy dispersive X-ray spectroscopy and X-ray photoelectron spectroscopy data clearly demonstrate the superior oxidative stability of the new electrolyte. The structural stability of the bulk cathode materials cycled with different electrolytes is extensively studied by X-ray absorption near edge structure and X-ray diffraction.

1. Introduction

Due to their many advantages, lithium-ion batteries (LIBs) have become the power sources for the consumer electronics and will potentially dominate large-scale energy storage application for electric vehicles.[1–6] To achieve high energy density required by the transportation application, an applicable approach is to increase the cell voltage and/or the cell capacity as indicated by the following equation $\Delta E = \int_0^{\Delta Q} V \cdot q\mathrm{d}q$, where E is the energy, V is the cell voltage, and q is the charge. Since the potentials of the lithiated graphite and lithiated silicon anode materials are close to that of the lithium metal, there is no space to further lower the anode potential, thus affording a high voltage cell. However, much could be explored on the cathode side such as enabling 5 V $LiNi_{0.5}Mn_{1.5}O_4$ and $LiCoMnPO_4$ cathodes. The traditional Ni-based layered oxide cathodes (for example, $LiNi_{1/3}Mn_{1/3}Co_{1/3}O_2$, NMC111) have a theoretical capacity of 287 mA h g^{-1} and their practical capacities are proportional to the charging voltages.[7–9] In particular, $LiNi_{0.5}Mn_{0.3}Co_{0.2}O_2$ (NMC532) is a promising high energy material due to its good electrochemical stability and high capacity at high voltages,[10–12] thus abstracting much attention in the academia and battery industry. However, new challenges associated with the low voltage stability of the state-of-the-art (Gen 2) electrolyte hinder the practical application of the high voltage high energy density LIBs cycled at cell voltages higher than 4.4 V.[13,14]

In a LIB, electrolyte plays a basic role in facilitating electrode redox reaction in the format of the Li^+ transfer back and forth between the electrodes and passivating the anodes (for example, graphite or silicon) to enable the reversible Li^+ intercalation/insertion. When the charging potential of the cathode is higher than the thermodynamically stable potential of the solvated electrolyte solvents, parasitic reactions occur leading to the decomposition of the electrolyte, loss of active lithium, and impedance rise on the electrode/electrolyte interface. Gen 2 electrolytes (for example, 1.2 M $LiPF_6$ in ethylene carbonate (EC)/ethyl methyl carbonate (EMC) 3/7 weight ratio) is anodically unstable when charging potential reaches over 4.5 V versus Li^+/Li.[3] At these high cutoff voltages, the cathode suffers from the irreversible oxygen evolution and resulting reactions with electrolyte solvents, and the high oxidation state active transition metal species (Ni^{4+} and Mn^{4+}) oxidizes the carbonate solvent by accepting electrons and the reduced species undergoes a disproportionation reaction leading to the dissolution of the transition metal ions in the electrolyte, especially Ni^{2+} and Mn^{2+}. These metal ions diffuse to the graphite anode surface getting reduced and catalyze further side-reaction of the electrolyte on the graphite anode causing the huge

M. He, Dr. C.-C. Su, Dr. P. Fenter, Dr. Z. Zhang
Chemical Sciences and Engineering Division
Argonne National Laboratory
9700 South Cass Avenue, Argonne, IL 60439-4837, USA
E-mail: zzhang@anl.gov

M. He, Dr. Y. Wang
Department of Mechanical Engineering
Worcester Polytechnic Institute
100 Institute Road, Worcester, MA 01609, USA

Prof. Z. Feng
School of Chemical, Biological, and Environmental Engineering
Oregon State University
Corvallis, OR, USA

L. Zeng, Prof. M. J. Bedzyk
Applied Physics Program
Northwestern University
Evanston, IL 60208, USA

Dr. T. Wu
X-Ray Science Division
Argonne National Laboratory
9700 South Cass Avenue, Argonne, IL 60439-4837, USA

Prof. M. J. Bedzyk
Department of Materials Science and Engineering
Northwestern University
Evanston, IL 60208, USA

DOI: 10.1002/aenm.201700109

impedance increase and active lithium loss.[15–18] Next generation of oxidation-stable electrolytes is in great demand to enable the electrochemical stability of the LIB when cycled at cell voltages higher than 4.4 V.

In recent years, our group has reported a fluorinated electrolyte[19–23] as promising substitute for the traditional carbonate electrolytes and demonstrated the impact of the fluorination on both the highest occupied molecular orbital (HOMO), the lowest unoccupied molecular orbital, and oxidation stability of the fluorinated carbonate solvents. Other groups also reported the fluorinated compounds as electrolyte additive. For example, Lee et al. reported that the addition of 5 wt% methyl(2,2,2-trifluoroethyl) carbonate (henceforth, FEMC) to 1.0 M $LiPF_6$ in EC/EMC (3/7 weight ratio) could improve the cycling performance as the FEMC can form a passivation layer and can prevent the transition metal from dissolution on the cathode material surface.[24] Another example by using the fluorinated compound for the high voltage cell is lithium difluoro(oxalato) borate (LiDFOB). Zhu and co-workers demonstrated that, by incorporating 2 wt% LiDFOB as an electrolyte additive,[25] the cell performance of Li-rich NMC/graphite cells was improved due to the formation of the solid-electrolyte-interface (SEI) at the anode electrode and passivation on the cathode preventing the transition metal dissolution.

Herein, we report a new fluorinated electrolyte formulation of 1.0 M $LiPF_6$ fluoroethylene carbonate (FEC)/bis(2,2,2-trifluoroethyl) carbonate (HFDEC) plus 1.0 wt% LiDFOB additive and demonstrated its superior performance in a 4.6 V LIB system with a Ni-rich cathode $LiNi_{0.5}Mn_{0.3}Co_{0.2}O_2$ (NMC532) coupled with a graphite anode. Beyond the enhanced oxidation stability, this fluorinated electrolyte met all other prerequisite requirements as an electrolyte such as high ionic conductivity, good separator and electrode wettability, and solid–electrolyte-interface[26] formation capability on graphitic surface.

Post-test analysis by scanning electron microscopy (SEM)/energy dispersive X-ray spectroscopy (EDS) indicated the cathode cycled with fluorinated electrolyte as much cleaner surface and less deposit of decomposition products on the graphite anode due to the suppression of transition metal (Mn^{2+}) dissolution, consistent with the X-ray photoelectron spectroscopy (XPS) data. Bulk electrode analysis via X-ray absorption spectroscopy (XAS) and synchrotron X-ray diffraction (SXRD) revealed that the fluorinated electrolyte facilitated the charging process for both Ni and Co in the NMC532 compared to Gen 2 electrolyte and preserved the intact crystal structure of NMC532 cathode. This systematic investigation of a fluorinated electrolyte in a Ni-rich NMC532 battery validates the rational design of the enhanced oxidation stability of the fluorinated electrolyte and proves to be an effective approach for high voltage electrolyte development for high energy density lithium ion battery for next generation electric vehicles.

2. Results and Discussion

Figure 1 summarizes the chemical structure and acronym of the fluorinated carbonate solvents, nonfluorinated carbonate solvents, lithium salt, and electrolyte additive used in this study. Fluorinated cyclic carbonate FEC, linear fluorinated carbonate HFDEC, and LiDFOB were synthesized in our lab and purified by fractional vacuum distillation and recrystallization prior use. 1.0 M $LiPF_6$ FEC/HFDEC (5/5 volume ratio) with 1.0% LiDFOB was formulated in the Argon-filled glove-box. Its conductivity was measured by AC impedance spectroscopy using a self-designed coin cell with a hollow Teflon disc with specific thickness and diameter. The detailed measurement and variable temperature conductivity data were provided in the Supporting Information.

2.1. Oxidation Stability Fluorinated Electrolyte

Substitution groups of fluorine (—F) on FEC molecule and fluorinated alkyl ($-CH_2CF_3$) on HFDEC molecule exert strong electron-withdrawing effect on the carbonate core and lower the HOMO energy level of the solvents based on the quantum chemistry simulation. Oxidation stability is the important criteria in designing high voltage electrolyte.[27,28] Linear sweep voltammetry (LSV) using an inert working electrode of platinum was first performed on the formulated fluorinated electrolyte and the Gen 2 electrolyte with a scan rate of 10 mV s^{-1}. **Figure 2** presents the LSV voltammograms covering the voltage window from 3 to 7 V versus Li^+/Li. The drastic increase of the oxidation current was observed for the Gen 2 electrolyte at 6.85 V indicating the main oxidative decomposition of the carbonate solvents. For the fluorinated electrolyte, the same oxidation current was observed at a delayed voltage of 7.05 V. Based on the density function theory calculation,[21] the theoretical oxidation potential of EC and EMC are 6.95 and 6.91 V, respectively. Comparatively, the oxidation potential of FEC and

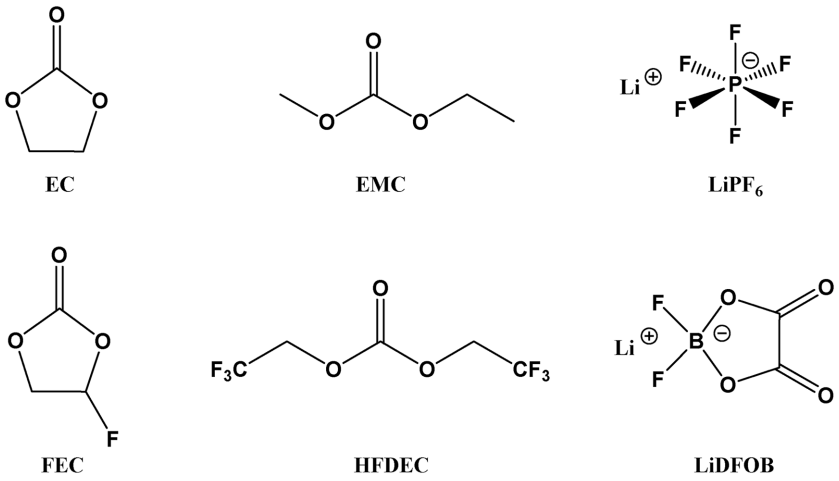

Figure 1. Chemical structures and acronym of carbonates, fluorinated carbonates, electrolyte additive, and lithium salt employed in this study (EC: ethylene carbonate, EMC: ethylmethyl carbonate, FEC: fluoroethylene carbonate, HFDEC: bis(2,2,2-trifluoroethyl) carbonate, LiDFOB: lithium difluoro(oxolato)borate and $LiPF_6$: lithium hexafluorophophate).

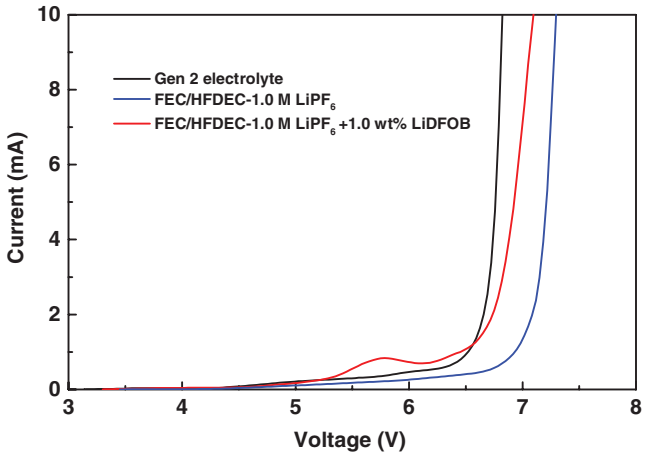

Figure 2. Linear sweep voltammograms of fluorinated electrolytes with a scan rate of 10 mV s^{-1}. Three-electrode cell with Pt (disc with a diameter of 2 mm) as working electrode and Li as reference and counter electrodes.

HFDEC were calculated to be 7.24 and 7.25 V, respectively, a 0.2–0.3 V higher than that of the Gen 2 electrolyte. It is noted that the oxidation potential obtained from the LSV experiment is significantly higher than that in the previous reports, 4.5 V versus Li^+/Li. That is because unlike a real cathode, which is an interactive transition metal rich surface, an inert platinum working electrode usually gives higher value of oxidation potential. The thermodynamic stability of the fluorinated electrolyte is expected to stabilize the cathode/electrolyte interface, thus suppressing the parasitic reactions causing ultimate transition metal ion dissolution.

2.2. Stable Cycling of a NMC532/Graphite Cell Charged to 4.6 V

In addition to the enhanced oxidation stability on an inert working electrode, the 1.0 M $LiPF_6$ FEC/HFDEC fluorinated electrolyte showed excellent performance in a NMC532/graphite full cell cycled at a rate of C/3 with voltage window from 3.0 to 4.6 V. **Figure 3**a,b shows the charge and discharge voltage profiles for the 1st, 10th, 25th, 50th, 75th, and 100th cycle for Gen 2 electrolyte and fluorinated electrolyte. It is manifested that the voltage polarization for both charging and discharging process increases significantly for Gen 2 cell,[29] while much less polarization was observed for fluorinated electrolyte cell, suggesting that higher resistance was built up at the electrode interface caused by the deposit of organic decomposition species of Gen 2 electrolyte.[18] Figure 3c shows the capacity retention for the first 100 cycles. The first charge and discharge capacities for Gen 2 cell are 248 and 214 mA h g^{-1} (86.4% Coulombic efficiency) and the capacity retention is 67% for 100 cycles. In contrast, despite lower first cycle efficiency (85.4%), the fluorinated electrolyte cell shows a capacity retention of 82% for 100 cycles, a significant improvement over Gen 2 cell even in such a limited cycle number. In a lithium-limited full cell, the capacity fading could be caused by

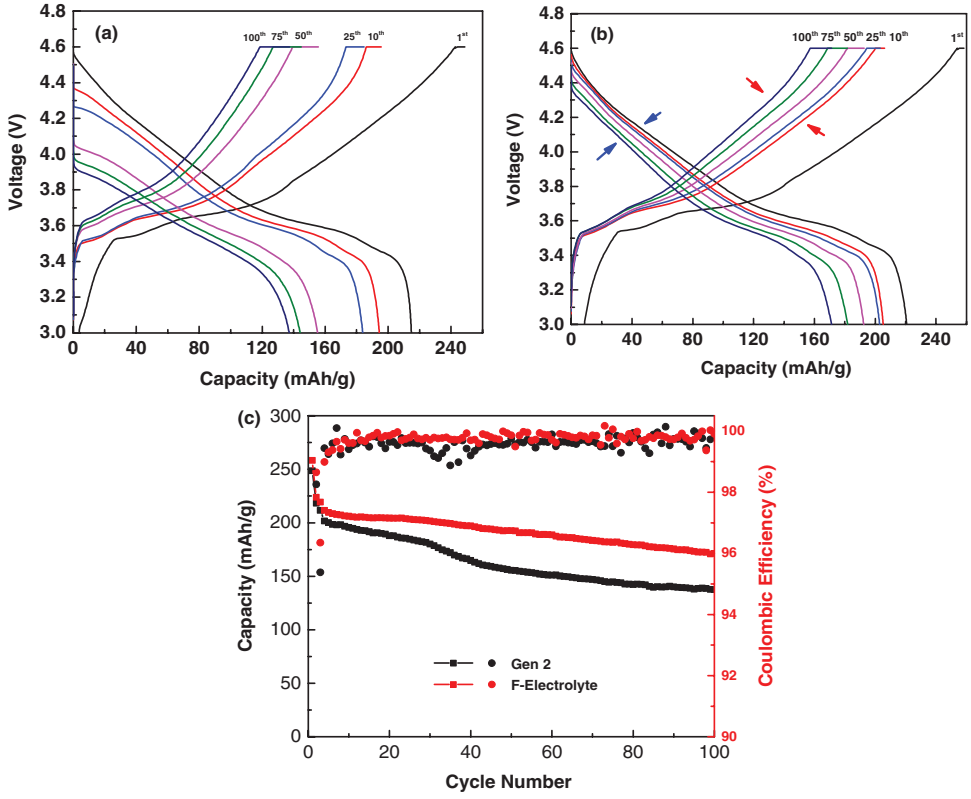

Figure 3. Voltage profiles for $LiNi_{0.5}Mn_{0.3}Co_{0.2}O_2$/graphite full cells in a) Gen 2 electrolyte, b) fluorinated electrolyte, and c) capacity retention and Coulombic efficiency (cycling condition: C/10 for two cycle formation and then C/3 for 100 cycles for cycling with 3.0–4.6 V cutoff voltage).

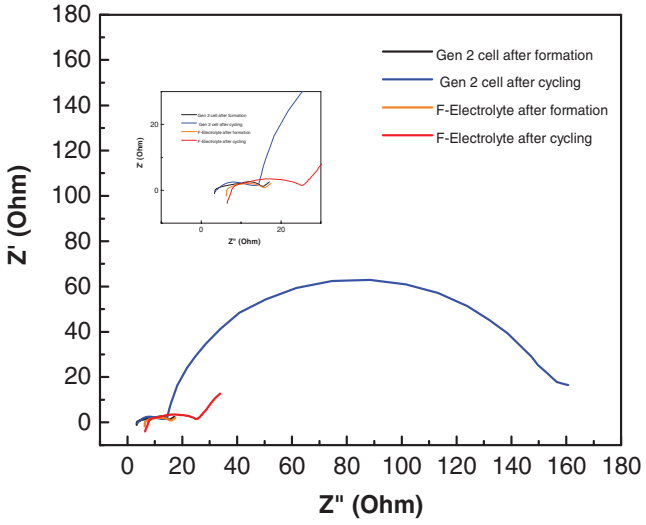

Figure 4. Electrochemical impedance spectra for $LiNi_{0.5}Mn_{0.3}Co_{0.2}O_2$/graphite cells after two-cycle C/10 formation step and 100-cycle C/3 repeated charge and discharge test (all impedance experiments were performed at fully discharged state).

the oxidative decomposition of electrolyte on charged cathode and/or the reductive decomposition on the lithiated anode. For the FEC-based fluorinated electrolyte, it proved to be compatible with graphitic anode due to the sufficient passivation by the reductive decomposition of FEC solvent.[22] In addition, an SEI formation additive LiDFOB was added to further assist the SEI formation from FEC, which accounts for the more loss of active lithium and thus lower first cycle Coulombic efficiency.[30–36]

To probe the interfacial impedance of the cycled cells, electrochemical impedance spectroscopy (EIS) was performed after the formation cycles and 100 cycles. As shown in **Figure 4**, the cells after formation cycles with Gen 2 and fluorinated electrolyte showed similar interfacial resistance and charge transfer resistance represented by the high frequency and mid frequency semicircles (inset in the figure), respectively.[2,37] However, after 100 cycles, the fluorinated electrolyte cell displayed significantly lower charge transfer resistances than the Gen 2 cell, suggesting that fluorinated electrolyte efficiently suppressed electrolyte breakdown on the surface of charged cathode surface. EIS results are in good agreement with the scanning electron microscope analysis. **Figure 5** showed the SEM images of the cycled NMC532 cathodes and cycled graphite anodes in two electrolytes and the pristine cathode (Figure 5a) and anode (Figure 5d). For the Gen 2 electrolyte cell, the morphologies of both cathode (Figure 5b) and anode (Figure 5e) were completely changed compared with the pristine electrodes and heavy decomposition of decomposition products were observed on both electrodes. However, little change in morphology was observed for the cycled cathode (Figure 5c) and cycled anode (Figure 5f) with fluorinated electrolyte. It is surprising that the cycled graphite anode in the fluorinated electrolyte almost resembles the pristine one (Figure 5a), confirming the effective passivation layer formed by fluorinated electrolyte. Since Gen 2 electrolyte forms excellent SEI on the graphite anode, the heavy deposition on the graphite surface is totally unexpected and new degradation mechanism must exist.

Figure 6 shows the EDS spectroscopy of the cycled graphite anodes. Two distinguished Mn peaks were observed in the EDS spectrum of the Gen 2 anode and the same species was also detected by the XPS Mn_{2P} spectroscopy as shown in **Figure 7**.

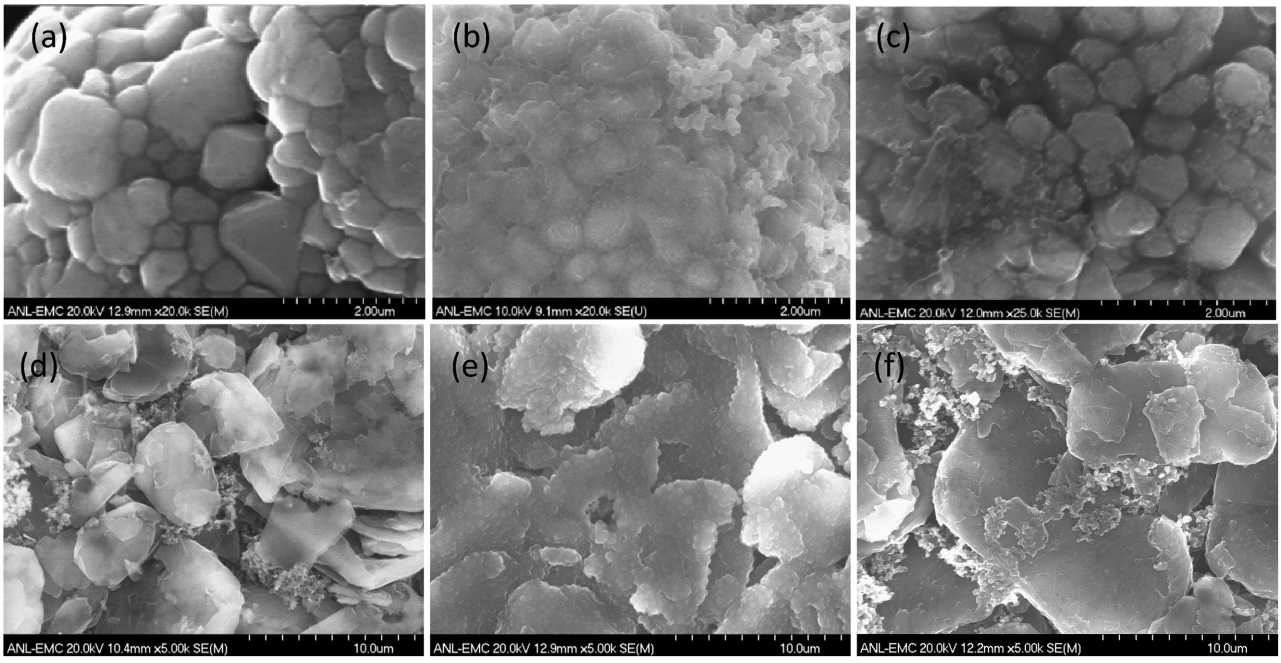

Figure 5. SEM images electrode at different stages: a) Pristine NMC532 cathode, b) cycled cathode with Gen 2 electrolyte, c) cycled cathode with fluorinated electrolyte, d) pristine anode, e) cycled anode with Gen 2 electrolyte, and f) cycled anode with fluorinated electrolyte. Magnification for cathode is higher than for anode in order to show the surface morphology change.

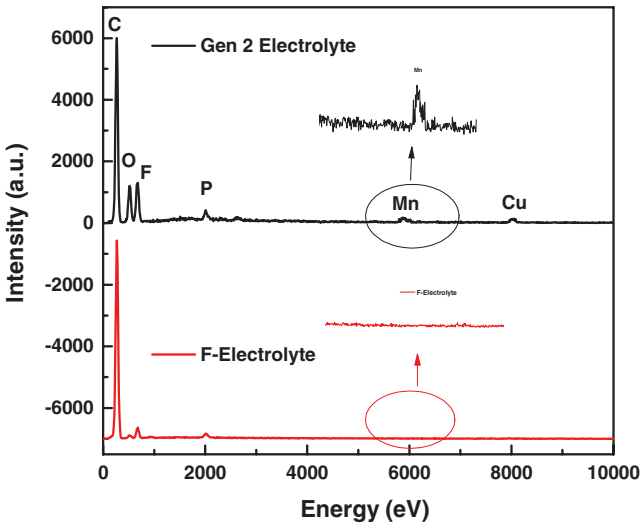

Figure 6. EDS spectra of the harvest graphite anode cycled with Gen 2 electrolyte (top black curve) and with fluorinated electrolyte (bottom red curve). Various spots on cycled anode were examined and are representative of the whole anode.

The deposition of Mn species on the cycled anode originated from the dissolution of the cathode active material, migration through the electrolyte, and deposition on the anode by forming the metal fluoride (MnF_2), metal oxide (MnO), or metal (Mn).[36,38] Moreover, the Mn plating catalyzes the electrolyte decomposition on the anode,[39] resulting in a thick electrolyte decomposition layer covering the surface of the anode. No Mn peaks were observed on the EDS spectrum (Figure 6, red curve) and XPS spectrum (Figure 7, bottom curve) of the fluorinated electrolyte cycled anode. C_{1s}, F_{1s}, and O_{1s} XPS data were included in the Supporting Information.

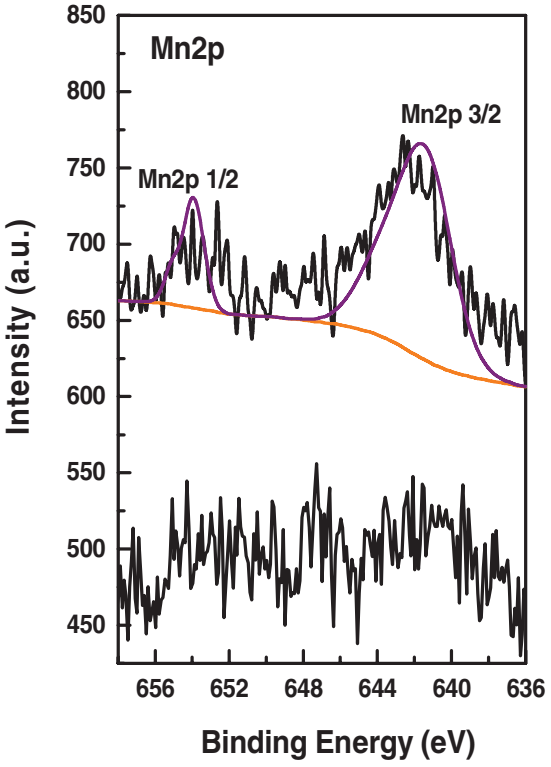

Figure 7. Mn_{2p} XPS spectrum for the harvested graphite anodes cycled in Gen 2 electrolyte and fluorinated electrolyte.

2.3. Cycled NMC532 Cathode Analysis

2.3.1. X-Ray Absorption Spectroscopy

To examine the electronic and local structure of transition metal in the cathode at different stages, ex situ XAS has been employed. Ni, Co, and Mn K-edge X-ray absorption near edge structure (XANES) as well as Fourier transformed extended X-ray absorption fine structure (EXAFS) of NMC532 cathode were carried out at pristine, fully charged (4.6 V), and discharge (3.0 V) states. The strong arising edge features are ascribed to the purely dipole-allowed 1s → 4p transition, which reflects oxidation state change of the transition metals. **Figure 8**a displays the Ni K-edge profiles of NMC532 at different stages. Figure S8a (Supporting Information) confirms that Ni in the pristine sample is Ni^{2+} referenced as the edge position of the standard NiO material. At discharged state, Ni K-edge XANES profile showed a slight shift to low energy when cycled with fluorinated electrolyte. The large change was observed at the fully charged state, Ni XANES edge shifts to higher energy for the fluorinated cycled cathode indicating that Ni reached higher oxidation state (Ni^{3+}/Ni^{4+}). This difference was caused by the low oxidation stability of the Gen 2 electrolyte which releases electron and compensates the charge on the Ni.[40] During the charging, most of the capacity was from Ni oxidation, as a result, Ni—O and Ni—M bond distance and coordination numbers are expected to change, which is evidenced from EXAFS spectra in Figure 8b. EXAFS spectra for the discharged material is nearly the same as the pristine, indicating that the local structures of NMC532 were maintained. However, at the charged state, the dramatic changes of the first coordination peaks indicate that the charge compensation mainly occurs at the Ni sites and results in significant alternations in the average Ni—O bond length. The large changes for the first Ni—O shell are caused by the Ni oxidation from Ni^{2+} to Ni^{4+} and also reported for the $Li_{1-x}Co_{1/3}Ni_{1/3}Mn_{1/3}O_2$ material by Yoon et al.[41] For fluorinated electrolyte cycled cathode, large shifts support the conclusion that Ni could be charged to higher oxidation state contributing more capacity.

For Mn K-edge XANES spectrum of pristine cathode, it is slightly on the right side of MnO_2 (Figure S8c, Supporting Information) suggesting the chemical state of Mn in NMC532 is $4 + \delta$, where δ refers to a small number close to zero. XANES spectra at charged state did not show a rigid shift to higher energy region with only a small change in the shape due to change in the Mn local environment. The energy position and the shape of Mn edges are very similar to those of the $Li_{1.2}Cr_{0.4}Mn_{0.4}O_2$ and $LiNi_{0.5}Mn_{0.5}O_2$ materials,[41] and similar trends of XANES spectra as a function of lithium concentration in $Li_{1-x}Ni_{0.5}Mn_{0.5}O_2$, which suggests that Mn remains at its original chemical state of $Mn^{(4+\delta)+}$ throughout the charge–discharge processes. This is also supported by previous studies on

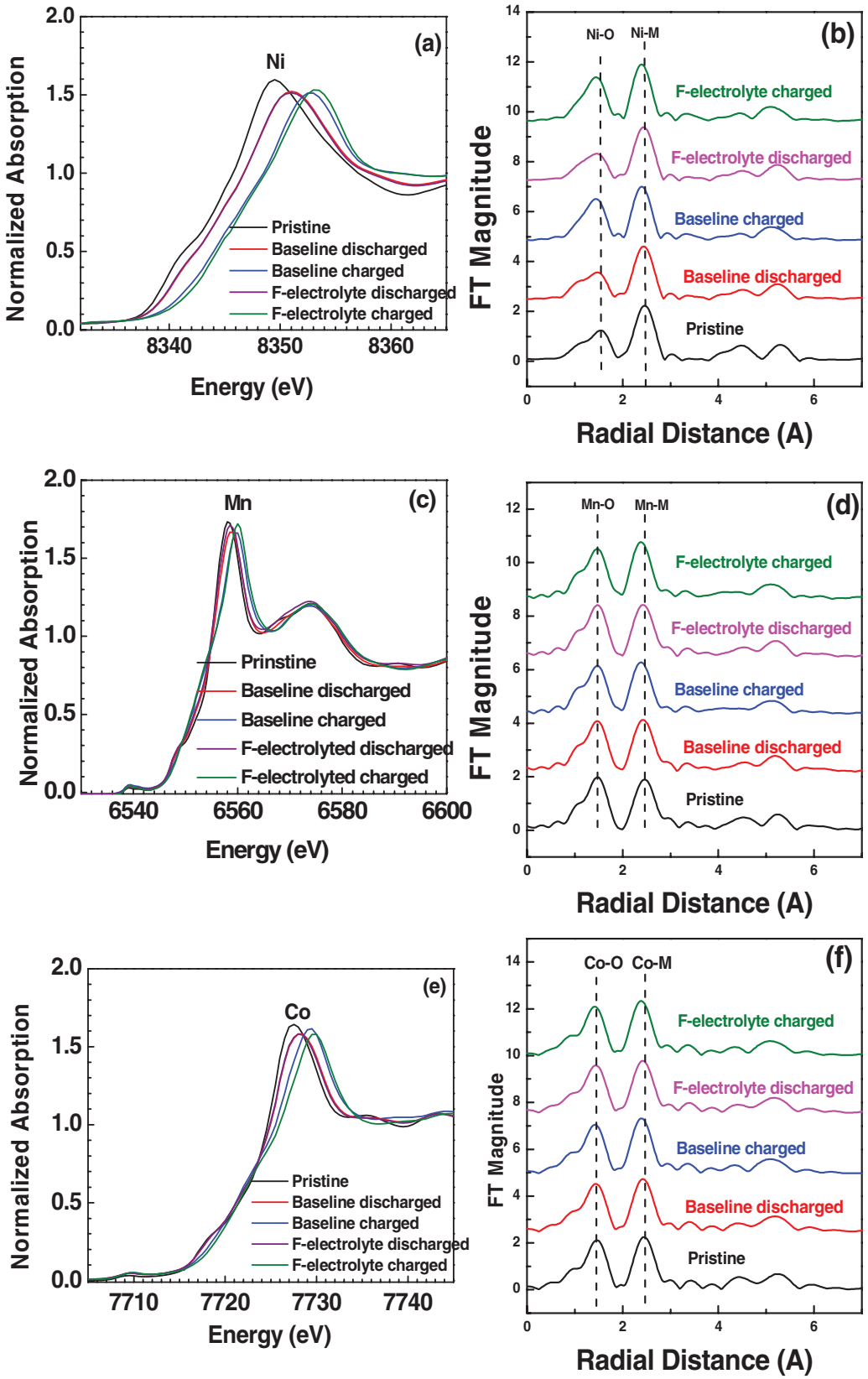

Figure 8. Normalized K-edge X-ray near edge structure (XANES) spectra at a) Ni K-edge, c) Mn K-edge, e) Co K-edge for NMC532 in pristine, charged (4.6 V) and discharged (3 V) states using Gen 2 and fluorinated electrolytes after 100 cycles, and b) Ni, d) Mn, and f) Co K-edge extended X-ray absorption fine structure (EXAFS) spectra for NMC532 in pristine, charged, and discharged states (note that the radial distances in EXAFS spectra have not been phase corrected).

Mn $L_{II,III}$-edge XAS.[41] From the EXAFS of the Mn K-edge in Figure 8d, the Mn—O bond length remains mostly unchanged during charge/discharge in both electrolytes; however, the Mn—M bond length (2 Å < R < 3 Å) during charge was shortened, as the peak position in this region becomes smaller. As the inert Mn does not change the bond distance between Mn and O during charge, the reduction of the Mn—M bond length could be ascribed to the reduction of the *a*-axis during charge processes.[40]

Figure 8e shows the K-edge XANES profiles of Co. The oxidation state of Co for the pristine cathode is approximately Co^{3+} as shown in the Figure S8b (Supporting Information). Similar with Ni, oxidation state of Co is nearly the same. One theoretical study for NMC111[42] indicated that Co^{3+}/Co^{4+} redox reaction would occur at fairly high potentials at high voltages. At 4.6 V, a slightly higher energy shift was observed for cobalt in the charge state, suggesting partial of Co involved in the redox reaction. Co involved more redox reaction when charged in fluorinated electrolyte than Gen 2 electrolyte as indicated by both the Co XANES spectra shape change and the bond length and covalency[41] from the EXAFS data shown in Figure 8f.

In summary, combined with the pre-edge data in Figure S6 (Supporting Information), both the Ni and Co cycled in the fluorinated electrolyte can be charged to higher oxidation state due to its intrinsic oxidation stability, thus contribute more capacity than Gen 2 electrolyte. Mn remains inert during the electrochemical reaction in both electrolytes. XAS experimental on Ni, Mn and Co K-edge infers the advantage of fluorinated electrolyte to promote and protect NMC during charge-discharge process.

2.3.2. Synchrotron X-Ray Diffraction Analysis

To examine the cathode structure cycled at high voltage, synchrotron X-ray diffraction analysis was performed on cathodes which were completely galvanostatically discharged with a small current (C/20) to 3.0 V prior the X-ray experiment. **Figure 9** shows the XRD diffraction patterns of the aluminum current collector, pristine and two cycled NMC532 electrodes in Gen 2 electrolyte and fluorinated electrolyte. Three NMC532 XRD patterns are in good agreement with a single phase $\overline{R}_{3m}$ $NaFeO_2$ structure and all the reflections can be indexed by assuming the hexagonal axes setting of the rhombohedral $\overline{R}_{3m}$ space group.[43] No new phases were detected by SXRD. The reflection pairs (006)/(102) and (108)/(110) are well resolved, a typical feature of a well-developed layered structure.[44]

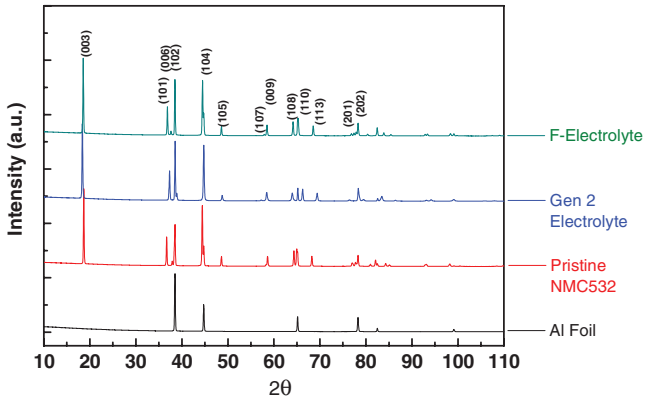

Figure 9. SXRD patterns of aluminum foil, pristine and cycled NMC532 electrodes in Gen 2 electrolyte and fluorinated electrolyte.

Table 1 summarizes the refinement data. Compared with the pristine material, NMC532 cycled in fluorinated electrolyte showed very little crystallographic changes, whereas the electrode cycled in the Gen 2 electrolyte shrank by 3% due to the contraction of *a*, *b* axis and the enlargement of *c* axis. The increase of *c* parameter is attributed to the loss of active lithium during cycling.[40] For the $LiMO_2$ (M = Ni, Co, Mn) material, the oxygen anions are in a close-packed arrangement in ABCABC framework with transition metal cations located in the six coordinated octahedral site. The transition metal slab and lithium layer are stacked alternatively.[9] The absence of lithium ions causes the expansion of the two negative charged oxide layers, leading to the increase of *c* parameter.[45–47] Ideally, the carbonate electrolytes are reduced during the initial cycles forming SEI on the anode electrode[48] and kinetically stabilizes the electrode/electrolyte interface.[49] However, this interface is changed under high voltage charging condition. As indicated by the EDS and XPS data shown in Figures 6 and 7, the electrolyte instability caused the transition metal dissolution in the electrolyte. During charging process, the Mn^{2+} dissolved in the electrolyte and diffused to the anode side getting reduced.[16] This process depleted active Li^+ by the following reaction[36]

$$MnF_2 + 2LiC_6 \rightarrow Mn + 2LiF + 2C_6 \quad (1)$$

LiF and Mn deposited on the surface of the graphite anode, which were well identified by the F_{1s} XPS spectroscopy in Figure S7 (Supporting Information), EDS in Figure 6, and Mn_{2p} XPS in Figure 7. Due to the loss of active lithium, the number of active lithium ion that can return to the cathode structure was reduced, which accounts for the change of cathode crystal parameter and the irreversible capacity during repeated cycling. To compensate the charge, the transition metal oxidation state is increased as evidenced by the XAS data shown in Figure 8. The bond length of Ni^{2+} is 0.69 Å and Co^{3+} is 0.61 Å, meanwhile, 0.56 Å for Ni^{3+} and 0.53 Å for Co^{4+}.[50] The higher valence state of transition metal leads to the shrinkage of *a* and *b* parameters as shown in Table 1. In contrast, the NMC532 electrode cycled in fluorinated electrolyte resembles the pristine material and crystal parameters keep almost unchanged. These results are consistent with XAS experiment data.

Table 1. Refined XRD lattice parameters *a*,*c* and cell volume for NMC532 cathodes cycled with Gen 2 electrolyte (Gen 2) And fluorinated electrolyte (F-electrolyte).

NMC523 cathode	Lattice parameters			V [Å^3]
	$a = b$ [Å]	c [Å]	c/a	
Pristine	2.866	14.8944	5.196	122.34
Gen 2	2.798	15.1494	5.083	118.60
F-electrolyte	2.871	14.8964	5.182	122.03

3. Conclusion

In this article, we report a fluorinated electrolyte based on 1.0 M $LiPF_6$ FEC/HFDEC with 1.0 wt% LiDFOB for the high voltage lithium ion battery. It met all the basic requirements as a non-aqueous electrolyte including graphite anode passivation, high conductivity, and excellent wettability with cell components. On top of these properties, this fluorinated electrolyte is oxidatively stable against high voltage charging and showed significantly improved cell performance when charged to 4.6 V in NMC532/graphite couple. Linear sweep voltammetry, repeated charge–discharge cycling, and a series of post-test analysis including SEM/EDS, XPS, XRD, and XAS confirm its voltage advantage over the Gen 2 electrolyte. Charge transfer impedance of the cell cycled with fluorinated electrolyte is much smaller than that cycled with Gen 2 electrolyte and significant depositions were detected on the both NMC532 cathode and graphite anode. Interestingly, the transition metal dissolution is not detected by EDS and XPS on the fluorinated electrolyte cycled graphite anode, suggesting the enhanced voltage stability on the cathode side and the robust SEI formation on the graphite anode. This has been evidenced from the XAS experiment confirming that the Ni and also Co could be charged to higher oxidation state (Ni^{3+}/Ni^{4+}) with fluorinated electrolyte due to its enhanced oxidation stability. Furthermore, fluorinated electrolyte was proved to assist the preservation of the crystal structure of NMC532 cathode by SXRD results. The lattice structure of NMC532 is almost intact while significant shrinkage in its unit cell for Gen 2 electrolyte cycled cathode. All results converge to the conclusion that FEC/HFDEC based fluorinated electrolyte is intrinsic ally stable toward oxidation and is suitable as high voltage electrolyte for high voltage high energy density lithium ion cell. This example research demonstrated that new electrolyte design could provide an approach to solve the technical barriers encountered by the high voltage high energy density lithium-ion batteries.

4. Experimental Section

Synthesis of HFDEC: The symmetric fluorinated linear carbonates were synthesized following the procedure published in ref. [21]. In a typical procedure for di-trifluoroethyl carbonate (HFDEC), 2,2,2-trifluoroethanol (18.5 g, 0.185 mol, 6.17 equiv), triethylamine (20.2 g, 0.2 mol, 6.67 equiv), and 4-dimethylaminopyridine (Sigma-Aldrich, 36 mg, 0.3 mmol, 1% mol) were mixed together in a round-bottom flask and cooled to 0 °C. A solution of triphosgene (8.9 g, 0.03 mol, 1 equiv) in CH_2Cl_2 was added into the mixture dropwise via a syringe pump over the course of 8 h. The mixture was then allowed to warm up to ambient temperature and stirred for 48 h. The reaction was then quenched with 1 N HCl, and the product was extracted with CH_2Cl_2 and washed further with HCl and then with brine solution. The crude product was distilled to remove CH_2Cl_2, dried with 4 Å molecular sieves, and then fractionally distilled twice to afford the pure product (99.1% by gas chromatography) with an isolated yield of 39% and 15 ppm water content as measured by Karl-Fischer titration. ^1H, ^{13}C, and ^{19}F-NMR spectra of HFDEC are shown in Figures S1–S3 (Supporting Information) and conductivity data of the formulated electrolytes were shown in Figure S4 (Supporting Information). Moreover, the wettability of the formulated electrolyte and baseline electrolyte are shown in Figure S5 (Supporting Information).

Electrolyte and Electrode Preparation: An electrolyte of 1.2 M $LiPF_6$ dissolved in EC and EMC in 3:7 ratio by weight, designated as Gen 2 electrolyte, was purchased from Tomiyama Pure Chemical Industries. FEC was purchased from Solvay and was purified by drying with 4 Å molecular sieve and vacuum distillation before use. The fluorinated electrolyte was prepared by dissolving 1.0 M $LiPF_6$ in FEC/HFDEC mixture solvent at 5/5 ratio by volume with 1.0 wt% LiDFOB as additive. The electrolyte preparation was performed in an Ar-filled glove-box with controlled moisture content <5 ppm. The cathode was made of 90 wt% NMC532, 5 wt% carbon black C45, and 5 wt% Solvay polyvinylidene fluoride (PVDF) 5130 binder coated on aluminum foil. The active material loading averaged 9.15 mg cm^{-2}. The graphite anode was made of 89.8 wt% Conoco Phillips CGP-A12, 4 wt% Super P-Li, 6 wt% Kureha PVDF 9300 binder, and 0.2 wt% oxalic acid coated on copper foil. The active material loading averaged 5.3 mg cm^{-2}. The effective diameters of cathode, anode, and separator were 14, 15, and 16 mm, respectively.

Electrochemical Evaluation: Linear sweep voltammetry was performed using a Pt/Li/Li three-electrode cell with a voltage window from 3 to 7 V at a scan rate of 10 mV s^{-1}. Galvanostatic charge–discharge cycling tests for NMC532/graphite coin cells (2032) were conducted on Maccor Electrochemical Analyzer (MIMSclient) with cutoff voltages 3.0 and 4.6 V at C/3 rate after two C/10 formation cycles.

Electrochemical Impedance Spectroscopy: Impedance measurements were tested at 30 °C that was maintained by an oven. The spectra were collected using a Solartron impedance analyzer in the frequency range from 1 MHz to 0.01 Hz, with an amplitude of 10 mV.

Electrode Morphology Characterization: The morphologies of the electrodes after cycling were investigated by SEM and energy dispersive X-ray spectroscopy[48] using a Hitachi S-4700-II microscope in the Electron Microscopy Center, Argonne National Laboratory.

Electrode Surface Analysis: The cycled cells were disassembled in the glove-box, and the electrodes were washed with anhydrous dimethyl carbonate to remove residual electrolyte and dried for overnight. X-ray photoelectron spectroscopy (XPS) measurements were carried out by using a Thermo Scientific ESCALAB 250Xi with Al Kα source. A low-energy electron flood gun was used to compensate for X-ray beam induced surface charging. C_{1s} peak (284.8 eV) was used for energy calibration.

X-Ray Diffraction Analysis: SXRD was performed to quantify the structure and compositions of electrode materials at beam-line 17-BM at the Advanced Photon Source (APS) at the Argonne National Laboratory using X-ray wavelength of 0.72768 Å. Samples were attached to Kapton tapes and measured in transmission mode. A PerkinElmer amorphous silicon flat panel detector was used to collect 2D XRD data. Integration of the 2D data to conventional plots of intensity versus 2θ, which was converted to a 2θ value at X-ray wavelength of 1.5406 Å (Cu Kα source) for the convenience of comparison with reference database.

X-Ray Absorption Analysis: X-ray absorption near edge spectroscopy and EXAFS experiments were carried out at beam-line 9BM-C of APS at the Argonne National Laboratory. The following electrode materials were used: pristine NMC532 (called pristine in the discussion), NMC532 cathodes discharged in Gen 2 electrolyte at 3 V (G2_3V) and charged at 4.6 V (G2_4.6 V) after 100 cycles, and NCM 523 cathodes discharged in fluorinated electrolyte at 3 V (F_3 V) and charged at 4.6 V (F_4.6 V) after 100 cycles. Samples were placed in a chamber with helium flow as the protection. All data were collected in transmission mode. A Lytle detector was used to collect all transition metal X (X = Ni, Mn, and Co) while the Si(111) monochromator scanned the incident X-ray photon energy through X K-edge absorption edge. The monochromator was detuned to 80% of the maximum intensity at X K-edges to minimize the presence of higher harmonics. The X-ray beam was calibrated using the corresponding transition metal foil K-edges, namely Ni, Mn, and Co foils. Data reduction and data analysis were performed with the Athena software packages. Standard procedures were used to extract the EXAFS data from the measured absorption spectra. The pre-edge was linearly fitted and subtracted. The postedge background was determined by using a cubic-spline-fit procedure and then subtracted. Normalization was performed by dividing the data by the height of the absorption edge at 50 eV.

Supporting Information

Supporting Information is available from the Wiley Online Library or from the author.

Acknowledgements

This research was supported by the Vehicle Technologies Office, U.S. Department of Energy. Argonne National Laboratory is operated by UChicago Argonne, LLC for the U.S. Department of Energy under contract DE-AC02-06CH11357. The authors would like to thank the Cell Analysis, Modeling, and Prototyping (CAMP) Facility of Argonne's Chemical Sciences and Engineering Division for providing the electrode materials.

Keywords

electrode/electrolyte interface, fluorinated electrolytes, $LiNi_{0.5}Mn_{0.3}Co_{0.2}O_2$ cathode, oxidation stability, post-test analysis

Received: January 11, 2017
Revised: February 13, 2017
Published online: April 26, 2017

[1] K. Xu, *Chem. Rev.* **2014**, *114*, 11503.
[2] M. He, X. Zhang, K. Jiang, J. Wang, Y. Wang, *ACS Appl. Mater. Interfaces* **2014**, *7*, 738.
[3] K. Xu, *Chem. Rev.* **2004**, *104*, 4303.
[4] K. Xu, A. von Cresce, *J. Mater. Chem.* **2011**, *21*, 9849.
[5] K. Xu, S. Zhang, T. R. Jow, W. Xu, C. A. Angell, *Electrochem. Solid-State Lett.* **2002**, *5*, A26.
[6] S. S. Zhang, *J. Power Sources* **2007**, *164*, 351.
[7] T. Ohzuku, A. Ueda, M. Nagayama, Y. Iwakoshi, H. Komori, *Electrochim. Acta* **1993**, *38*, 1159.
[8] M. N. Ates, Q. Jia, A. Shah, A. Busnaina, S. Mukerjee, K. Abraham, *J. Electrochem. Soc.* **2014**, *161*, A290.
[9] T. Ohzuku, Y. Makimura, *Chem. Lett.* **2001**, *30*, 642.
[10] J.-Z. Kong, C. Ren, G.-A. Tai, X. Zhang, A.-D. Li, D. Wu, H. Li, F. Zhou, *J. Power Sources* **2014**, *266*, 433.
[11] S. Liu, L. Xiong, C. He, *J. Power Sources* **2014**, *261*, 285.
[12] R. Malini, U. Uma, T. Sheela, M. Ganesan, N. Renganathan, *Ionics* **2009**, *15*, 301.
[13] M. Nagahama, N. Hasegawa, S. Okada, *J. Electrochem. Soc.* **2010**, *157*, A748.
[14] X.-G. Sun, C. A. Angell, *Electrochem. Commun.* **2005**, *7*, 261.
[15] G. Assat, C. Delacourt, D. A. Dalla Corte, J. M. Tarascon, *J. Electrochem. Soc.* **2016**, *163*, A2965.
[16] N. P. Pieczonka, Z. Liu, P. Lu, K. L. Olson, J. Moote, B. R. Powell, J.-H. Kim, *J. Phys. Chem. C* **2013**, *117*, 15947.
[17] K. Nelson, D. Abarbanel, J. Xia, Z. Lu, J. Dahn, *J. Electrochem. Soc.* **2016**, *163*, A272.
[18] M. Xu, L. Zhou, Y. Dong, Y. Chen, J. Demeaux, A. D. MacIntosh, A. Garsuch, B. L. Lucht, *Energy Environ. Sci.* **2016**, *9*, 1308.
[19] Z. Zhang, L. Hu, H. Wu, W. Weng, M. Koh, P. C. Redfern, L. A. Curtiss, K. Amine, *Energy Environ. Sci.* **2013**, *6*, 1806.
[20] A. Benmayza, W. Lu, V. Ramani, J. Prakash, *Electrochim. Acta* **2014**, *123*, 7.
[21] M. He, L. Hu, Z. Xue, C. C. Su, P. Redfern, L. A. Curtiss, B. Polzin, A. von Cresce, K. Xu, Z. Zhang, *J. Electrochem. Soc.* **2015**, *162*, A1725.
[22] L. Hu, Z. Zhang, K. Amine, *Electrochem. Commun.* **2013**, *35*, 76.
[23] L. Hu, Z. Xue, K. Amine, Z. Zhang, *J. Electrochem. Soc.* **2014**, *161*, A1777.
[24] Y.-M. Lee, K.-M. Nam, E.-H. Hwang, Y.-G. Kwon, D.-H. Kang, S.-S. Kim, S.-W. Song, *J. Phys. Chem. C* **2014**, *118*, 10631.
[25] X. Xin, X. Zhou, F. Wang, X. Yao, X. Xu, Y. Zhu, Z. Liu, *J. Mater. Chem.* **2012**, *22*, 7724.
[26] I. Buchberger, S. Seidlmayer, A. Pokharel, M. Piana, J. Hattendorff, P. Kudejova, R. Gilles, H. A. Gasteiger, *J. Electrochem. Soc.* **2015**, *162*, A2737.
[27] S. Zhang, T. Jow, *J. Power Sources* **2002**, *109*, 458.
[28] H. Lee, S. Choi, S. Choi, H.-J. Kim, Y. Choi, S. Yoon, J.-J. Cho, *Electrochem. Commun.* **2007**, *9*, 801.
[29] L. Lu, X. Han, J. Li, J. Hua, M. Ouyang, *J. Power Sources* **2013**, *226*, 272.
[30] D. Aurbach, B. Markovsky, G. Salitra, E. Markevich, Y. Talyossef, M. Koltypin, L. Nazar, B. Ellis, D. Kovacheva, *J. Power Sources* **2007**, *165*, 491.
[31] J. Shim, R. Kostecki, T. Richardson, X. Song, K. A. Striebel, *J. Power Sources* **2002**, *112*, 222.
[32] D. Aurbach, B. Markovsky, A. Rodkin, E. Levi, Y. Cohen, H.-J. Kim, M. Schmidt, *Electrochim. Acta* **2002**, *47*, 4291.
[33] J. B. Goodenough, K.-S. Park, *J. Am. Chem. Soc.* **2013**, *135*, 1167.
[34] V. Etacheri, R. Marom, R. Elazari, G. Salitra, D. Aurbach, *Energy Environ. Sci.* **2011**, *4*, 3243.
[35] T.-H. Cho, M. Tanaka, H. Onishi, Y. Kondo, T. Nakamura, H. Yamazaki, S. Tanase, T. Sakai, *J. Power Sources* **2008**, *181*, 155.
[36] S. B. Chikkannanavar, D. M. Bernardi, L. Liu, *J. Power Sources* **2014**, *248*, 91.
[37] B. Xu, D. Qian, Z. Wang, Y. S. Meng, *Mater. Sci. Eng., R* **2012**, *73*, 51.
[38] S. S. Zhang, *J. Power Sources* **2006**, *162*, 1379.
[39] M. He, C.-C. Su, C. Peebles, Z. Feng, J. G. Connell, C. Liao, Y. Wang, I. A. Shkrob, Z. Zhang, *ACS Appl. Mater. Interfaces* **2016**, *8*, 11450.
[40] C. F. Petersburg, Z. Li, N. A. Chernova, M. S. Whittingham, F. M. Alamgir, *J. Mater. Chem.* **2012**, *22*, 19993.
[41] W.-S. Yoon, M. Balasubramanian, K. Y. Chung, X.-Q. Yang, J. McBreen, C. P. Grey, D. A. Fischer, *J. Am. Chem. Soc.* **2005**, *127*, 17479.
[42] L. Wang, J. Li, X. He, W. Pu, C. Wan, C. Jiang, *J. Solid State Electrochem.* **2009**, *13*, 1157.
[43] X. Zhang, W. Jiang, A. Mauger, F. Gendron, C. Julien, *J. Power Sources* **2010**, *195*, 1292.
[44] S. K. Jung, H. Gwon, J. Hong, K. Y. Park, D. H. Seo, H. Kim, J. Hyun, W. Yang, K. Kang, *Adv. Energy Mater.* **2014**, *4*, 1300787.
[45] H. Q. Pham, K.-M. Nam, E.-H. Hwang, Y.-G. Kwon, H. M. Jung, S.-W. Song, *J. Electrochem. Soc.* **2014**, *161*, A2002.
[46] Y. Zhu, Y. Li, M. Bettge, D. P. Abraham, *J. Electrochem. Soc.* **2012**, *159*, A2109.
[47] M. Xu, L. Zhou, L. Hao, L. Xing, W. Li, B. L. Lucht, *J. Power Sources* **2011**, *196*, 6794.
[48] M. Herstedt, D. P. Abraham, J. B. Kerr, K. Edström, *Electrochim. Acta* **2004**, *49*, 5097.
[49] P. Arora, R. E. White, M. Doyle, *J. Electrochem. Soc.* **1998**, *145*, 3647.
[50] K. Shizuka, T. Kobayashi, K. Okahara, K. Okamoto, S. Kanzaki, R. Kanno, *J. Power Sources* **2005**, *146*, 589.

